Adsorption of emerging contaminants by graphene related materials and their alginate composite hydrogels

Journal of Environmental Chemical Engineering 11 (2023) 109566

Contents lists available at ScienceDirect

Journal of Environmental Chemical Engineering

journal homepage: www.elsevier.com/locate/jece

Adsorption of emerging contaminants by graphene related materials and their alginate composite hydrogels

Francesca Tunioli [a], Sara Khaliha [a], Sebastiano Mantovani [a], Antonio Bianchi [a], Alessandro Kovtun [a], Zhenyuan Xia [a,b], Mohammad Sajad Sorayani Bafqi [c], Burcu Saner Okan [c], Tainah Dorina Marforio [d,e], Matteo Calvaresi [d,e], Vincenzo Palermo [a,b], Maria Luisa Navacchia [a], Manuela Melucci [a,*]

[a] Consiglio Nazionale delle Ricerche, Institute for Organic Synthesis and Photoreactivity (CNR ISOF), via Piero Gobetti 101, 40129 Bologna, BO, Italy
[b] Industrial and Materials Science, Chalmers University of Technology, 41258 Göteborg, Sweden
[c] Sabanci University Nanotechnology Research and Application Center, SUNUM, Tuzla, Istanbul 34956, Turkey
[d] Alma Mater Studiorum - University of Bologna, Department of Chemistry 'G. Ciamician', via Selmi 2, 40129 Bologna, Italy
[e] Center for Chemical Catalysis – C3 Alma Mater Studiorum – Università di Bologna via Selmi 2, 40126 Bologna, Italy

ARTICLE INFO

Editor: Xin Yang

Keywords:
Graphene related materials
Polymer-graphene composites
Water purification
Emerging contaminants
Alginate

ABSTRACT

Graphene nanosheets and nanoplatelets -alginate composite hydrogels were prepared by ionic gelation and the resulting gel beads were exploited for the removal of a mixture of eight selected emerging contaminants (ECs) in tap water, including bisphenol A, ofloxacin and diclofenac. The role of graphene related materials (GRM) on the gel bead structure, adsorption selectivity, kinetic, mechanism, and efficiency was investigated. Combined Scanning Electron Microscopy (SEM) and confocal Raman microscopy mapping showed a porous structure with pore size in the range of 100–200 μm and a homogeneous distribution of graphene nanosheets or nanoplatelets at the pores surface. The adsorption kinetic of GRM was much faster than that of granular activated carbon (GAC), the industrial sorbent benchmark, with removal capacity of ofloxacin from 2.9 to 4.3 times higher. A maximum adsorption capacity of 178 mg/g for rhodamine B was estimated by adsorption isotherm studies for reduced graphene oxide-based beads (a value comparable to that of powered activated carbon). Regeneration test performed on saturated beads by washing with EtOH, and subsequent reiterated reuses, showed no loss of adsorption performance up to the fourth reuse cycle.

1. Introduction

The development of new materials and technologies for the removal of emerging contaminants (ECs) from drinking water is one of the current research priority to comply with the Sustainable Development Goal number 6 of the United Nations 'Ensuring clean water and sanitation for all', and to help water utilities and operators adopting the new European drinking water directive 2020/2184 [1,2].

ECs include thousands of products used for personal- health care (detergents, pharmaceuticals and cosmetics), and industrial uses (pesticides, plastic additives, etc.) [3,4]. The treatment of such contaminants generally relies on adsorption (i.e. on activated carbons), membrane filtration (i.e. ultrafiltration) or reverse osmosis (RO), or the combination of both technologies, i.e. in domestic point-of-use systems [5]. RO is currently the most efficient technology for high-performance water purification and desalination, with very high removal for several classes of contaminants, but its use is bound to some main drawbacks, such as elevated energy consumption needed to force water through the membrane, rejection of the inlet water (still close to 50%), and production of concentrate retentates, which need further treatment or disposal [6].

Adsorption through granular activated carbon (GAC) remains the most exploited strategy in potabilization plants, as last treatment step for the removal of trace contaminants before the final disinfection steps [7].

Integration of GAC with new, sustainable materials, with wider adsorption versatility toward organic and inorganic contaminants and increased capacity would be particularly advantageous for prolonging the GAC life-time or expanding the range of its applications.

* Corresponding author.
E-mail address: manuela.melucci@isof.cnr.it (M. Melucci).

https://doi.org/10.1016/j.jece.2023.109566
Received 24 December 2022; Received in revised form 8 February 2023; Accepted 21 February 2023
Available online 23 February 2023

Among carbonaceous nanomaterials, GRM have the largest surface area and adsorption capacity and are commercially available at good and reproducible standard.

Moreover, the tunable surface chemistry [8–14] and processability in 3D structures [15] make them particularly appealing for the development of advanced multifunctional materials [16–18]. The use of nanosheets is the best option to exploit the whole adsorption potential of graphene, but it requires a further microfiltration step to retain the exhausted nanosheets from treated waters [11,19]. Despite the increasing use of ultrafiltration and microfiltration in multi-train water treatments, the adjustment costs faced by drinking water treatment plants to implement adsorption and/or microfiltration treatments in drinking water production would be too demanding. The engineering of composites, such as membranes, foams, aero-hydrogels, based on porous polymers and GRM, appear as a more convenient and most ready-to-market alternative to exploit graphene in the water purification scenario [20,21].

We have recently reported on the development of polysulfone-graphene hollow fibers [22–24] and granules, [25,26] as well as on chitosan-graphene sponges, for the removal of ECs in drinking water and on the comparison of the adsorption mechanisms and performance between graphene embedding and graphene coating approaches [24,27]. We demonstrated that in all of these composites, adsorption was enabled by the exposure of the graphene nanosheets to the contaminated water. Both embedded and coated structures were active on the removal of different families of pollutants, such as organic contaminants (ofloxacin, ciprofloxacin, bisphenol A, etc), heavy metals (Pb, Cr(III), Cu), and polyfluoroalkyl substances (PFASs). Notably, graphene-based composites showed adsorption capabilities comparable to or even higher than GAC. For example, polysulfone-graphene hollow fibers showed a performance from 3 to 7 times higher than GAC in the removal of PB, Cr (III), Cu, and short chain PFAS [23].

Here, we report on alginate graphene composite gel beads synthesized by ionic gelation [28], embedding different types of GRM (Fig. 1a), i.e. graphene oxide (GO), reduced graphene oxide (rGO), graphene nanoplatelets (GNP), and graphene oxide covalently modified with lysine (GO-Lys) [29,30].

Alginate is a low cost natural polymer with high processability, widely used for realizing porous gel for adsorption studies [31–33].

On the other hand, the rationale behind GRM selection is their different surface chemistry that is expected to promote different contaminant-nanosheets interactions and the resulting final adsorption properties. GO and rGO have different oxidation ratios with consequent different number of oxygen groups (O/C=0.38 and 0.01, respectively, see Table S1), and surface charge (-43.1 ± 2.4 mV and -35.3 ± 3.1 mV, respectively). GO-Lys has a more positive surface charge (-35.2 ± 0.8 mV) [28] and slightly higher reduction rate than GO (O/C=0.17), while GNP have an even higher reduction degree (O/C=0.05) and a non-planar shape, with later size comparable to GO-based materials. Overall, these peculiarities are expected to influence the adsorption as well as the properties of their alginate composites [19].

The resulting different surface charge, hydrophilicity and water dispersibility of the GRM are expected to lead to different composite structures (i.e. filler distribution, pore size), ultimately affecting the kinetic, selectivity, and capacity performance.

The alginate gel beads prepared by using the different GRM were used as sorbent for the removal of a selection of eight organic contaminants from spiked tap water (Fig. 1.b).

It has been already demonstrated that the encapsulation of GO into a sodium alginate matrix has made the resulting composite material more porous and introduced stabilizing CO bonds between GO and alginate [34]. The adsorption of such composites of Cd (II), Cu (II) and Pb (II), and ciprofloxacin (CIPRO) from aqueous solutions by alginate-graphene beads has been demonstrated [35–37]. The tuning of GO amount as well as GO prefunctionalization was tested to enhance the adsorption capacity. On this line, M. Majdoub et al. showed that hexamethylenediamine (HMDA) covalent binding on GO led to remarkably high adsorption rates for Pb (II), Cu (II) and Cd (II), with only 15 wt% of GO-HMDA incorporated into the alginate beads, in both single contaminant or mixture solutions in tap water [36].

Similarly, amino post-functionalization of alginate shell increased its

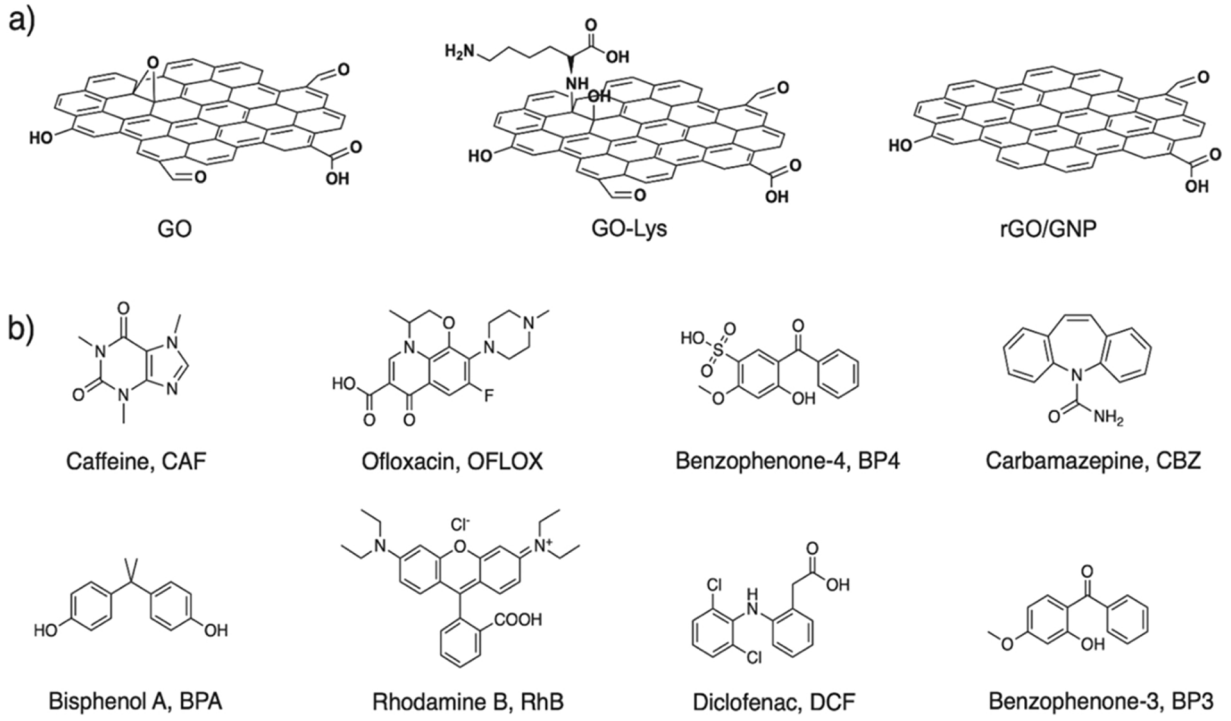

Fig. 1. (a) Simplified chemical structure of GRM used in this work, from left to right: graphene oxide (GO), GO covalently modified with lysine (GO-Lys), reduced graphene oxide (rGO) and graphene nanoplatelets (GNP); (b) chemical structure of the selected emerging contaminants (ECs).

maximum adsorption capacity (expressed in mg/g) by 130% and 182% towards Cu (II) and CIPRO, respectively [38].

Here, by a combined theoretical and experimental approach, we report the systematic investigation of the role of graphene type on the adsorption of several contaminants in their mixture. The removal of a mixture of emerging contaminants, in comparison to standard GAC, the regeneration and reuse of the presented composites are also discussed.

2. Materials and methods

2.1. Materials

GO was purchase from LayerOne (Norway) and used without further purification (graphene oxide powder <35 mesh, product code 1.8). rGO was purchased from LayerOne (Norway) and used without further purification (rGO powder, fully reduced, carbon content of about 98.5–99 wt%). GAC was purchased from CABOT Norit Spa (Ravenna, Italy, Norit GAC 830 AF, MB index min 240 mg/g, BET surface area >1000 m^2/g). Lysine-modified GO (GO-Lys) was synthesized by microwave-activated amination and purified by an innovative microfiltration protocol [28]. GNP was obtained from pyrolyzed waste tires provided by NANOGRAFEN Co. (Gebze, Kocaeli, Turkey) and use without further purification. Further information about GRM are shown in ESI (Section S1). All chemicals were purchased from Sigma-Aldrich in the highest available purity and were used without any further purification.

2.2. Preparation of alginate-graphene beads

Alginate-graphene beads were obtained by ionic gelation, according to previously reported methods [28]. 100 mg of GRM (GO, rGO, GNP or GO-Lys) were dispersed in 50 mL of ultrapure water and then sonicated for 2 h. After that, 500 mg of sodium alginate were added to the suspension under magnetic stirring until a dense and homogeneous solution was obtained. The suspension was added dropwise into 150 mL of a 0.2 M $CaCl_2$ solution under gentle magnetic stirring and kept at room temperature for 12 h, to avoid beads aggregation. Finally, the hydrogel beads were washed 3 times with water and stored in ultrapure water at room temperature. The content of water was estimated by firstly weighting the beads (externally dried with filter paper), then drying them in the oven (80 °C, 24 h) and weighting them once again.

2.3. Structure characterization

Chemical composition of GRM was studied by using X-ray photoelectron spectroscopy (XPS), the results and the experimental details were reported in ESI (Section S1). The morphology of alginate-graphene beads was studied by SEM after cryo-cutting. The samples were frozen in liquid nitrogen, cut, and then lyophilized to remove water and maintain the original morphology of the beads. The cross section was coated with gold (Lecia EM ACE600) and observed by SEM (JEOL JSM-7800 F Prime) at an acceleration voltage of 8 kV. The GRM distribution inside the alginate matrix was studied by Raman confocal mapping performed on a confocal Raman micro-spectroscope (Alpha300R, WITec, Germany). The light source used was a 532 nm laser with the output power of around 0.7 mW cm^{-2}. The diffraction grating of 600 g/mm was employed together with a 50x microscope objective. A 2 mm step size was used in the *x* and *y* direction for each Raman image with 0.5 s integration time and a spectral range from 0 to 3600 cm^{-1}.

2.4. Kinetic-selectivity experiments

25 mg of powder materials (GO, rGO, GNP, GO-Lys) were sonicated in 5 mL of ultrapure water for 2 h. The resulting suspensions were added to 20 mL of the mixture of eight organic contaminants (final concentration 0.5 mg/L each in tap water). For non-powder materials (GAC, Alg, Alg-GO, Alg-rGO, Alg-GNP, Alg-GO-Lys), 25 mg of samples were added directly to 25 mL of the mixture of organic contaminants (concentration 0.5 mg/L each in tap water). Samples were then left in darkness under gentle agitation for 24 h. During this time, 200 μL withdrawals were collected after contact times of 15 min, 1 h, 4 h, and 24 h. Each sample was centrifugated (10 min, 10000 rpm) and analyzed with HPLC.

2.5. High performance liquid chromatography analyses

HPLC analyses of the selected mixture of eight contaminants were performed on a Dyonex Ultimate 3000 system equipped with a diode array detector. 200 μL samples were used as sources for the automated injection. The chromatographic separation was performed on a reverse phase Zorbax XDB-C8 column (4.6 × 150 mm^2, 5 μm) at flow rate of 1.0 mL/min, detection at λmax of each analyte, linear gradient TFA 0.05% aqueous solution/acetonitrile from 80:20–0:100. In each experiment, the removal of each analyte was determined by comparison with that of the initial untreated solution. The results are expressed as the mean of two independent experiments ± SD.

2.6. Release test

The release tests were performed on the same alginate-graphene beads used for kinetic experiments. After adsorption, beads were externally dried on filter paper to remove excess water and placed in 25 mL of clean tap water. The samples were kept in darkness under gentle stirring. After 4 h, 200 μL of solution were withdrawn and analyzed by HPLC to check the possible release of the adsorbed contaminants.

2.7. Molecular dynamic simulations

A 40 Å × 40 Å graphene sheet was used to model GO, rGO and GO-Lys. The functional groups attached to the different graphene sheets (epoxy, hydroxyl, carbonyl, and carboxylic acid, lysine) were randomly positioned to reproduce the experimental XPS data. The GAFF force field [39] was used to parametrize BP4 and RhB molecules, and graphene nanosheets. QM calculations (HF/ 6–31 G(d)), followed by RESP fitting provided the atomic charges of BP4 and RhB. All the simulations were carried out in an explicit solvent box (using the TIP3P water model). Counterions were added to neutralize the system. Molecular dynamic simulations (MD) were carried out using AMBER 16 [40]. After equilibration, 100 ns MD simulations were produced. The binding affinity of BP4 and RhB to GO, rGO and GO-Lys were calculated by using the molecular mechanics–generalized Born surface area (MM-GBSA) method [41] extracting the snapshots from the MD trajectories.

2.8. Adsorption isotherms

The adsorption isotherms on different GRM and alginate-graphene beads were performed on RhB at a fixed amount of adsorbent material and by varying the contaminant concentration (see details in ESI, Table S2-S8). In a total volume of 5 mL of ultrapure water, RhB at different concentrations was added to the sorbent materials (powder materials were previously sonicated for 2 h in ultrapure water). The solutions were kept in darkness under gentle stirring for 24 h and then analyzed by UV-Vis spectroscopy (Agilent Cary 3500). Experimental data were fitted by Langmuir and BET models; the plots, the equation, and the R2 are shown in ESI (Table S9-S10, Fig. S4). For BET model, the saturation concentrations (Cs) was optimized during the fit, selecting 1 mg/mL as the maximum value (maximum RhB solubility experimentally determined).

2.9. Regeneration test

Alginate-graphene beads (25 mg) were placed in 25 mL of an RhB solution (5 mg/L, tap water). Samples were kept in darkness under gentle stirring (RhB has low photostability). After 24 h, the solutions were analyzed by UV-Vis spectroscopy. The same beads were externally dried on filter paper to remove excess water, placed in 25 mL of EtOH for 24 h and the solution analyzed by HPLC to check possible release. The beads were recollected and washed in water (25 mL, for 30 min) and then reused in a new adsorption step. The procedure adsorption-washing-reuse was repeated for four times.

3. Results and discussion

3.1. Preparation and characterization of alginate-graphene beads

The gel beads were prepared by ion exchange. Briefly, GO/GO-Lys/rGO/GNP powders were sonicated in ultrapure water, then sodium alginate was added in ratio 5:1 w/w (alginate:GRM) to the suspension, under magnetic stirring. The dense dispersion was added dropwise into a $CaCl_2$ solution and then left at room temperature, collected, washed, and stored in ultrapure water. The so obtained composites beads are shown in Fig. 2.

A percentage of water (w/w) between 97% and 98% was estimated for all each type of bead (Alginate: 97.9%, Alg-GO: 97.2%, Alg-GO-Lys: 97.8%, Alg-rGO: 97.1%, Alg-GNP: 96.9%).

The stability of the beads was proved by UV-Vis analysis of the suspensions at different aging times. After ten days, the suspensions were still clear (Fig. 2c). UV-Vis analysis showed no evidence of signals deriving from nanosheets release. Fig. 2d shows also the spectrum of a GO standard suspension at 2.5 mg/L, proving that release of GO nanosheets did not occur at this limit of detection.

The chemical composition of GRM used in this work was studied by XPS and data are in agreement with previously reported ones [29,42]. The oxidation degree of the studied materials (expressed as O/C) decreased in the following order: GO (0.38) > GO-Lys (0.17) > GNP (0.05) > rGO (0.01) (details in table S1, ESI).

The spatial distribution of GRM inside the composite beads, and their morphology, were studied by combining scanning electron microscopy (SEM) and Raman confocal mapping. For these analyses, gel beads were prepared by cryo-cutting. SEM analyses (Fig. 3) of all samples showed the typical micrometric porous structure of alginate hydrogel with a dense skin layer.

Raman spectra of alginate and alginate-graphene beads are shown in Fig. 4a. All samples containing GRM showed two characteristic peaks at 1350 and 1596 cm^{-1}, respectively the D band (defects and disorders) and the G band (pristine sp^2 carbon atoms). The G band did not overlap with other characteristic peaks of alginate (2937 cm^{-1}, 1414 cm^{-1}, 1093 cm^{-1}), [43] allowing the study of the GRM distribution inside alginate matrix by Raman mapping. Fig. 4b-f shows the Raman 2D mapping and the relative optical images. As expected, pristine alginate samples did not show any G peak signal, due to the absence of GRM (Fig. 4b). Alg-GO and Alg-GO-Lys showed an almost homogeneous distribution of GRM at the edges of pores section, evidence of success in embedding graphene in the alginate matrix.

The Alg-rGO was still present along the whole edge, but in some part, as revealed by G signal near the edges, a broader spatial distribution was visible, suggesting the occurrence of aggregations. Among all of the GRM, GNP showed more inhomogeneous distribution inside Alg-GNP, with some regions with no signal at all and other with intense and large spots, showing sign of local agglomeration (Fig. 4f) and the highest G peak intensity (1E4 CCD cts).

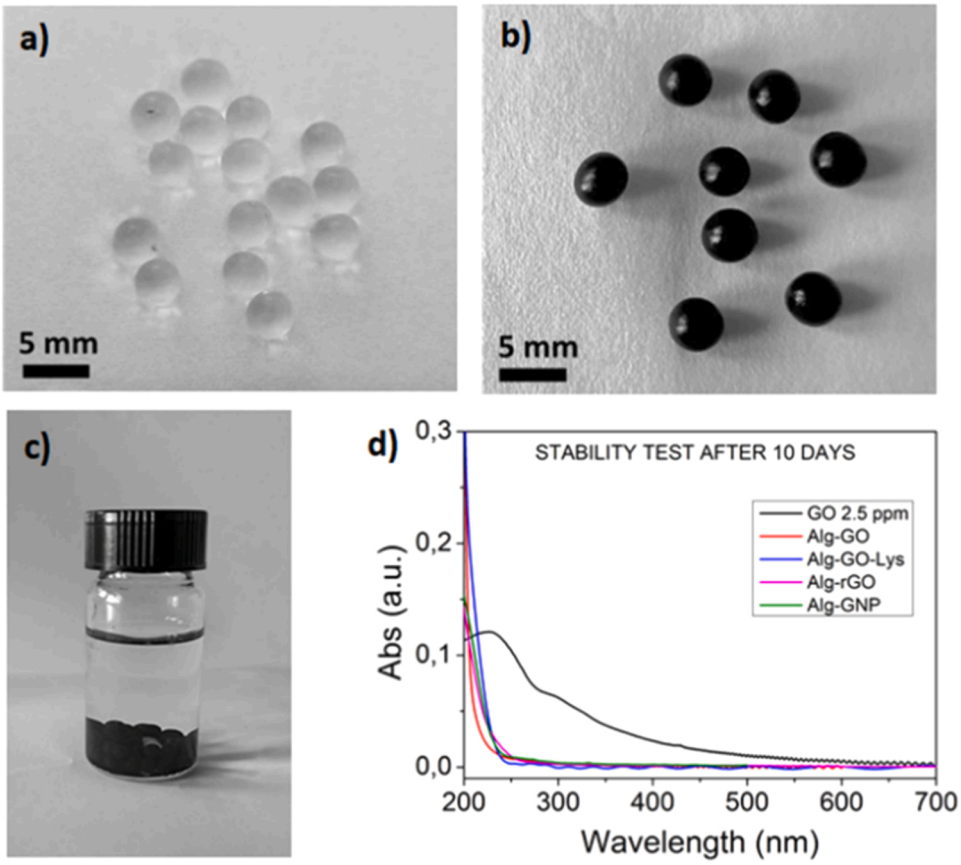

Fig. 2. (a) Alginate beads and (b) alginate-graphene beads; (c) stability test of composite beads in mQ water and d) corresponding UV-Vis spectra of solution after 10 days, in comparison to the spectrum of a 2.5 mg/L GO suspension (black line).

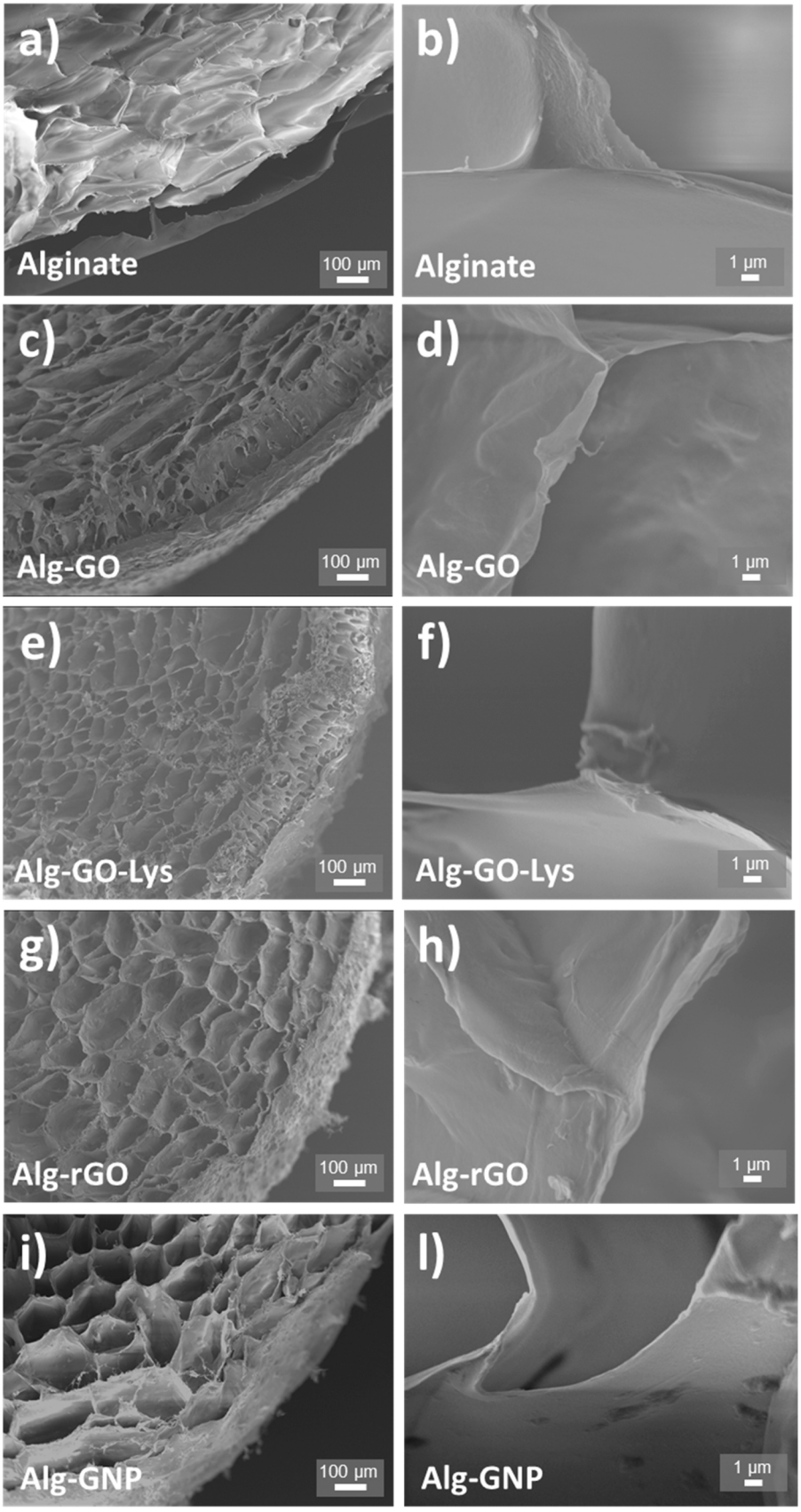

Fig. 3. Low and high magnification SEM cross-section images of (a,b) alginate, (c,d) Alg-GO, (e,f) Alg-GO-Lys, (g,h) Alg-rGO, (i,l) Alg-GNP beads.

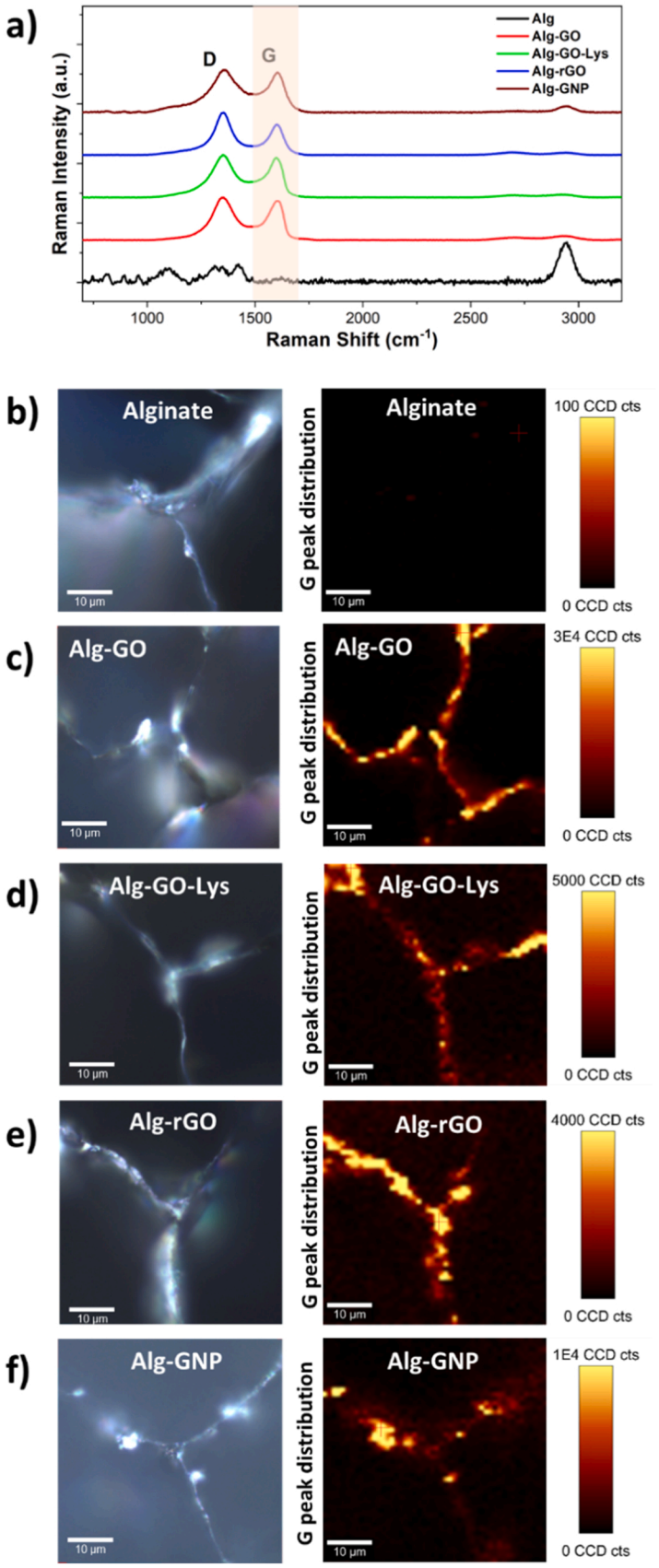

Fig. 4. (a) Raman spectra of alginate and alginate-graphene beads; (b-f) optical images and relative 2D Raman maps of used composites, constructed by using the G-band region.

3.2. Kinetic, selectivity and release experiments

The removal performances of GRM and of alginate and alginate-graphene gel beads toward the selected contaminant mixture at 15 min, 1 h, 4 h, and 24 were studied. At each contact time, an aliquot of treated water was analyzed by HPLC and the results at 1 h and 24 h are shown in Fig. 5 (data at 15 min and 4 h are reported in ESI, Fig. S2).

It can be seen that within the first hour of treatment rGO, GNP, and GO-Lys nanosheets outperformed GAC for almost all contaminants, with GAC becoming competitive only at 24 h (in the range 4–24 h, Fig. S2b and Fig. 5b). GO showed a lower performance than the other GRM for CAF, BP4, CBZ, BPA, and DCF. With the exception of CAF, the removal capability of GO remained almost unchanged for these compounds, even at equilibrium conditions (assumed here at 24 h).

Similar selectivity was observed for alginate beads (Fig. 5c-d and Fig. S2c-d), indicating that adsorption of the selected contaminants is mainly driven by GRM. Alginate showed almost negligible adsorption, while the performance of beads doped with GO, rGO, GNP, or GO-Lys increased with contact time. Alg-rGO and Alg-GO-Lys showed high removal after 24 h, with values above 80% for all contaminants. Alg-GNP showed slightly lower adsorption, with removal values ranging between 60% and 99%. As for the free nanosheets, Alg-GO showed lower performances for CAF, BP4, CBZ, and BPA (removal in the range of 5–15%), while effectively removed the other contaminants. The kinetics of the beads was significantly slower than those of the pristine GRM.

Indeed, for the composites, the equilibrium time ranges between 4 h and 24 h while for GRM most of the adsorption occurred within the first hour and slight increase was found at 24 h. The exfoliated nanosheets expose their whole surface area and are fully available for adsorption. On the other hand, in the composite beads the graphene adsorption sites are distributed in the in-active alginate matrix, this lowering the accessibility of the molecules to the graphene sorption sites ultimately increasing the time required for the adsorption.

The stability of the adsorption of all contaminants on GRM and on alginate composites were tested. To this aim, alginate-graphene gel beads used for the adsorption experiments, thus loaded with the contaminants, were washed and then left in fresh tap water for 4 h. Fig. S3, reported in ESI, shows the ratio between mass adsorbed and released for each contaminant. For Alg-GO-Lys and Alg-rGO, the release was below the limit of detection of the analytical method (~0.025 mg/L) for all contaminants. Only in the case of CBZ release of about 10% was found (Fig. S3b-c). Similarly, Alg-GO showed release of CAF and BP3 of 77% and 8% respectively (Fig. S3a). Alg-GNP showed the higher release with values up to 10–20% for CAF, BP4, CBZ and BPA (Fig. S3d). Collectively these results highlighted a stable adsorption of almost all contaminants on alginate-graphene composites.

To gain an insight on the adsorption mechanisms driving the observed selectivity we performed molecular dynamic simulations (MD) on the adsorption of BP4 and RhB on GO, rGO and GO-Lys. RhB and BP4 contaminants were selected for their markedly different chemical features, i.e. BP4 is representative of bent shaped, small size and neutral molecule (CAF, CAF, BP4, CBZ, BPA, and DCF) while RhB is large sized, flat aromatic (as OFLOX) and amphiphilic molecule. The three sorbents were selected to unravel the different role of chemical surface groups (i.e. -OH, -COOH or NH_2 Lys pendant groups) on the adsorption of the contaminant molecules. Fig. 6a shows representative snapshots from MD simulations of the favorite adsorption sites of BP4 and RhB on the GO, rGO and GO-Lys while the values of computed total binding affinity (E_{TOT}) are listed in Fig. 6b.

It is interesting to note that the lower adsorption of BP4 by GO shown in Fig. 5 corresponds to the lowest binding affinity calculated by MD (Fig. 6). The rough surface of GO, due to the surface oxygen groups likely minimize the interaction with these contaminants and limits the adsorption affinity which increases in the case of rGO having smoother nanosheets surface than GO. Nevertheless, for GO-Lys, the Lys adsorption sites on the nanosheets increase the binding affinity with BP4 enhancing its removal capacity respect to pristine GO.

For large molecules such as RhB, due to their large contact area,

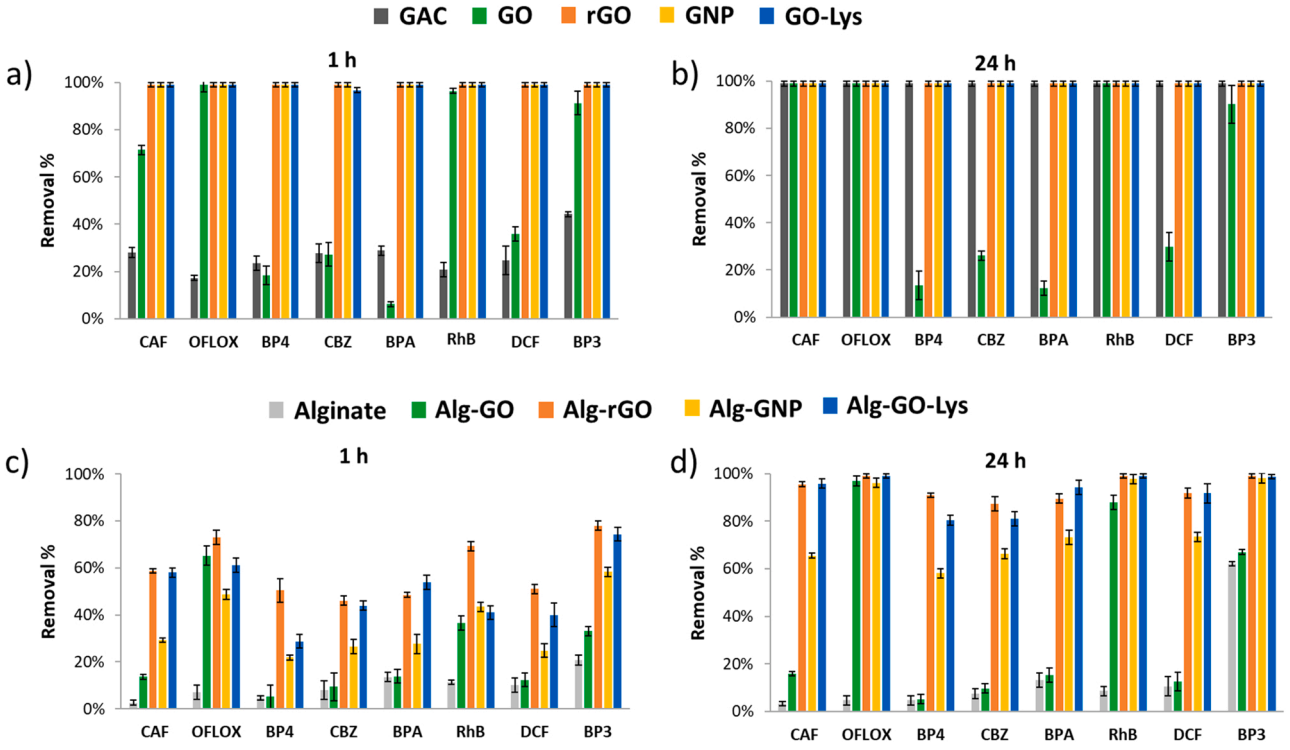

Fig. 5. Removal of ECs mix (0.5 mg/L each in tap water, Vtot= 25 mL, 25 mg of sorbent material). On the top, graphene nanosheets removal compared with GAC obtained after contact time of (a) 1 h, and (b) 24 h. On the bottom, alginate-graphene beds removal compared with pristine alginate beads after contact time of (c) 1 h, and (d) 24 h. Data at 15 min, and 4 h are reported in ESI, Fig. S2.

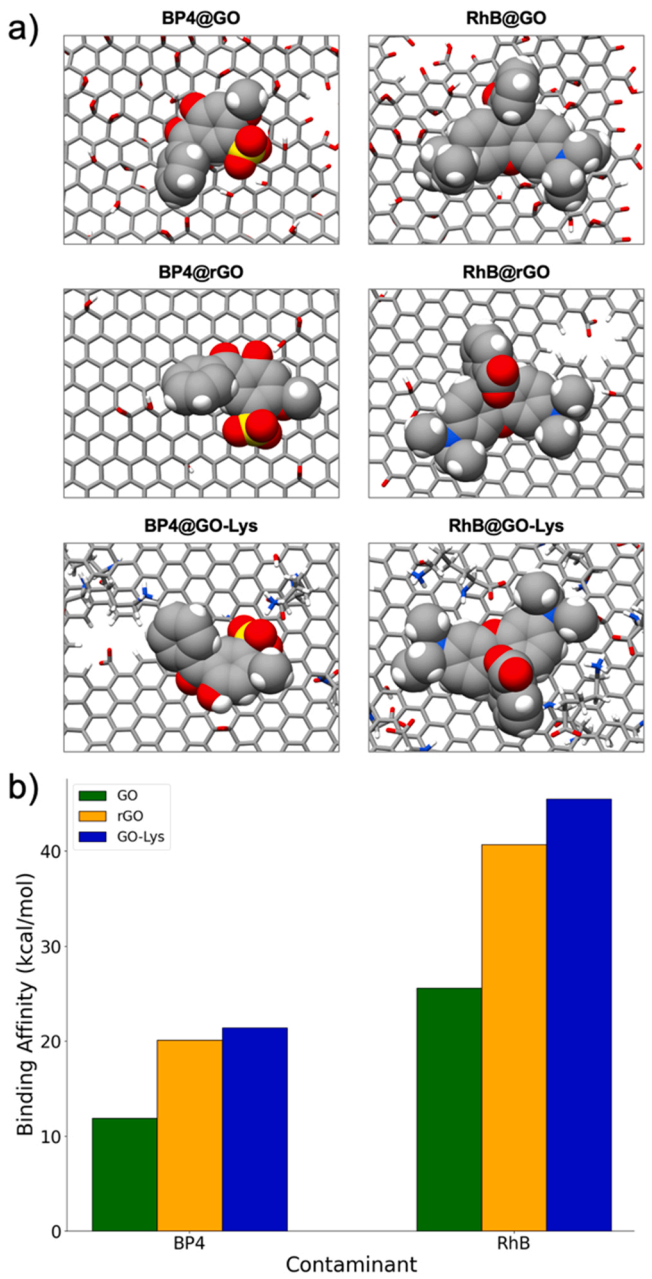

Fig. 6. (a) Representative snapshots from MD simulations of the favorite adsorption sites of BP4 and RhB on the GO (top), rGO (in the middle) and GO-Lys (bottom); (b) bar graph representation of the binding affinity for BP4 and RhB towards GO, rGO and GO-Lys. All energies are reported in kcal/mol.

adsorption is efficient with all the typologies of the nanosheets.

Collectively, the observed selectivity can be ascribed to the complex interplay of nanosheets exposed surface area (as shown by comparison GO vs rGO for BP4) and chemistry (as shown by the comparison GO vs GO-Lys for BP4).

3.3. Adsorption isotherms

The adsorption mechanisms and maximum monolayer capacity (Qm) of alginate-graphene beads were studied by adsorption isotherms experiments, which were carried out also for the pristine GRM on RhB (Fig. 7 and Fig. S4). RhB was selected as case study for its easy detection by UV–vis analysis and lowest limit of quantification respect to the other molecule and it allows the comparison of performance with respect to already reported materials. Adsorption isotherms were measured and fitted using two different models: i) Langmuir model, which describes an adsorption process with strong molecule-substrate interaction, where molecules are adsorbed in a single monolayer; and ii) Brunauer–Emmett–Teller (BET) model, describing a multilayer adsorption mechanism, where molecule-molecule interaction is comparable to the molecule-substrate one. It is notable that the adsorption of RhB on pristine nanosheets and composite beads were described by the same models, suggesting that the adsorption is driven by GRM, with a negligible role of alginate in molecule-substrate interaction.

GO-Lys and GNP adsorption was described by Langmuir model while BET model explained the adsorption data of GO and rGO, reported in a previous work. [11].

The maximum monolayer adsorption capacity (Qm) was obtained from the above reported model. Remarkably, we observed that Qm increased with the oxidation degree of the GRM (rGO: 220 mg/g < GO-Lys: 312 mg/g < GO: 439 mg/g, Table 1 and Table S1 in ESI). This trend can be explained in terms of the interplay between hydrophilicity and swelling, which influence the effective surface area available for adsorption. The driving force of the sorption for RhB on GRM are π-π interactions, which are deeply related to the accessible surface area of the 2D materials. [11] Oxidized and hydrophilic GRM (i.e. GO) swell in water, this increasing the nanosheets surface available for the adsorption of molecules at higher extent, with respect to hydrophobic materials, which are unable to swell. On the other hand, the relatively lower performance observed for GNP (68 mg/g) was ascribed to their poor water dispersibility, which causes aggregation. Moreover, GNP are a 3D structures formed by several layers of graphitic carbon, which cannot swell in water, contrarily to GO. This leads to a consequent physical lack of surface area exposed to the RhB molecules in water.

The adsorption on beads showed an unexpected behavior since the Qm decreases with the oxidation degree for GO, GO-Lys, and rGO, contrarily to the increase observed for pristine nanosheets (Fig. 8).

This phenomenon could be related to the inner morphology of the beads and to the dispersion homogeneity of the GRM inside the alginate matrix. Thanks to its high hydrophilicity, GO was homogeneously incorporated in the alginate beads. In contrast, the more hydrophobic rGO nanosheets, were segregated at the composite edges during the bead formation (as confirmed by Raman 2D mapping showed in Fig. 4). Fig. 9 shows a sketch of the nanosheets distribution in the porous structure of the alginate matrix. GO is well dispersed inside the matrix, while rGO is aggregated at the pore edges. Therefore, in Alg-GO, the GO nanosheets exposed to the water-pore interface (i.e. the active ones) were less than those exposed by Alg-rGO beads. This explains the remarkably higher adsorption capacity of Alg-rGO, compared to Alg-GO (178 mg/g and 15 mg/g, respectively). Lower water solubility and exposed surface area can also explain the trend observed for Alg-GNP, having GNP a heterogeneous distribution on the alginate beads surface (see Fig. 4f).

Nevertheless, the Qm values of Alg-rGO and Alg-GO-Lys (178 mg/g and 158 mg/g, respectively) are comparable to the values reported in literature for powder active carbon (Qm= 191 mg/g), the benchmark for dyes adsorption. [44] Moreover, comparing our composites with other materials proposed in literature for RhB adsorption, the Qm obtained from Alg-rGO and Alg-GO-Lys was one order of magnitude higher than nano Zn–Al–Fe_3O_4 blended alginate/Ca beads [45] (Qm=28 mg/g) and duolite C20 resin [46] (Qm=29 mg/g), and was comparable to the value obtained from an activated sugar-based carbon (Qm=123 mg/g). [47].

3.4. Regeneration test

The possible regeneration and reuse of alginate-beads was tested on RhB removal. RhB was selected as case study because of its easy detection by UV–vis spectroscopy. The initial concentration of RhB was higher than the values expected in real polluted water matrix to allow

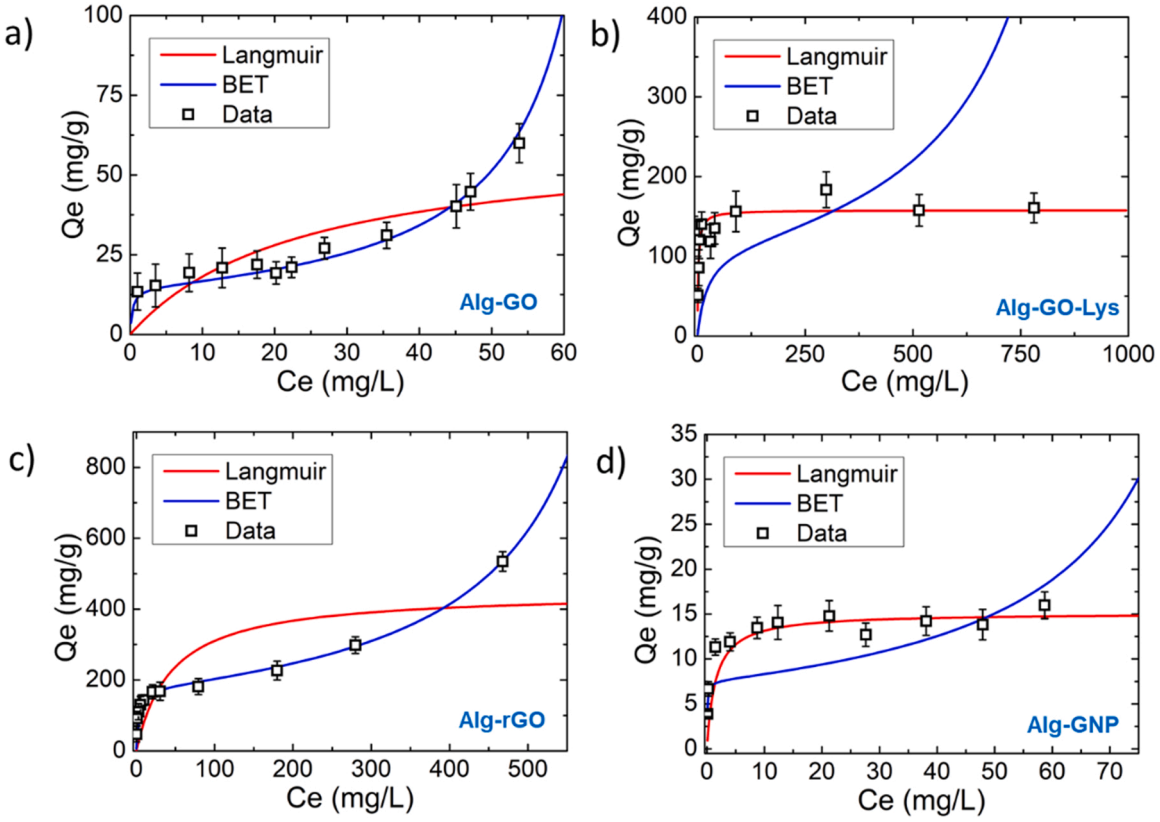

Fig. 7. Adsorption isotherm of (a) Alg-GO, (b) Alg-GO-Lys, (c) Alg-rGO, (d) Alg-GNP. (0.5 mg of sorbent, 24 h, 5 mL of RhB solution at different concentration). Data referred to GO-Lys and GNP nanosheets and pristine alginate beads are reported in ESI, Fig. S4.

Table 1
Maximum adsorption capacity (Qm) of RhB on different GRM and composite obtained from the fit of isotherms.

Material	NANOSHEETS: Qm (mg/g)	BEADS: Qm (mg/g)	Model fitting
GO	439*	15	BET
GO-Lys	312	158	Langmuir
rGO	220*	178	BET
GNP	68	15	Langmuir
Alginate	-	0.6	Langmuir

* from ref 11

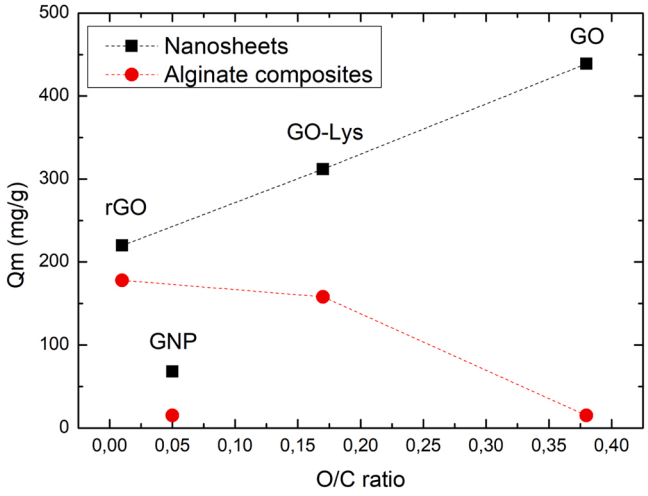

Fig. 8. Monolayer adsorption capacity (Qm) of RhB as a function of the oxidation degrees expressed as O/C ratio (rGO: 0.01, GNP: 0.05, GO-Lys: 0.75, GO: 0.38).

fast saturation of the sorbents. Five consecutive cycles of RhB adsorption and desorption were performed, in both cases we studied the system once it has reached the equilibrium, while, for practical application, we expect shortest contact time and reasonably lower performances. The removal efficiency of composite beads after each cycle is shown in Fig. 10. Beads were placed in contact with a solution of RhB (5 mg/L in tap water) for 24 h, then EtOH was used to wash saturated beads and remove RhB. This cycle was repeated five times without any loss in removal efficiency and any damage on the gel bead's structure. The control experiment, that consists only in a sequential use of beads with no use of EtOH, shows a monotonic decline of adsorption performances (see Fig. S5 reported in ESI) after just few cycles in all alginate-graphene composites. Concluding, by observing in detail the trends in Fig. 10, for Alg-GO and Alg-GNP the regeneration efficiency slowly decreases after each cycle, while the best performances was found for Alg-rGO and Alg-GO-Lys, that are always fully regenerated.

4. Conclusions

In this work, four types of GRM (GO, GO-Lys, rGO, GNP) were effectively incorporated in alginate matrix by ionic gelation to form porous composites that were exploited as sorbent for water remediation. Morphological characterization confirmed the successful retention of the alginate porous structure after GRM embedding with the nanomaterials exposed at the section edges of the pores. Efficient adsorption of all the eight tested contaminants with removal around 99% was observed for GO-Lys, rGO, GNP. On the other hand, GO showed high removal (>99%) toward all contaminants except for bent shaped molecules (BP4, CBZ, BPA and DCF) which were removed with efficiency in

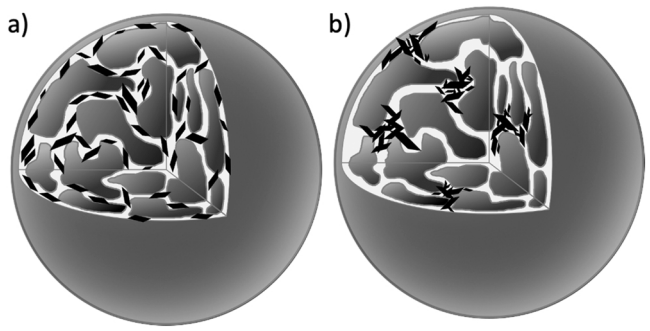

Fig. 9. Sketch of (a) Alg-GO and (b) Alg-rGO beads. The figure highlights the distribution of GO and rGO nanosheets in the porous structure of alginate matrix.

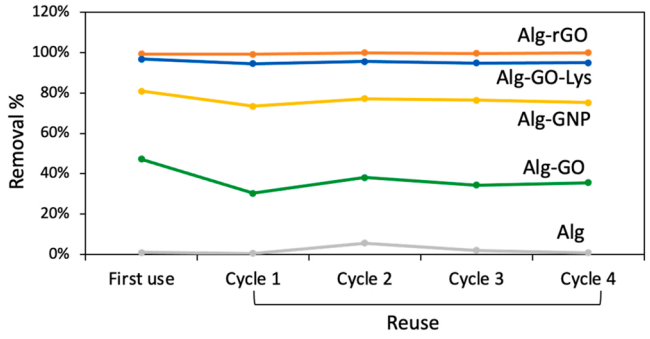

Fig. 10. Regeneration test on alginate and alginate-graphene beads. Each cycle includes an adsorption step (25 mg of beads, 25 mL of RhB, 5 mg/L in tap water, 24 h) and a desorption step (beads in 25 mL of EtOH, 24 h).

the range 12–30%. Similar selectivity was found for the alginate composites with higher removal observed for OFLOX, RhB and BP3 (removal up to 99%). The composites showed slower adsorption with respect to GRM likely due to the lowest active areas exposed by the composites respect to the free nanomaterials. Molecular modeling ascribed the observed selectivity to a complex interplay of molecules-graphene surface interactions with total energy binding values for large flat molecules such as RhB with respect to small and bent molecules such as BP4.

Remarkably, both GRM and alginate composites outperformed GAC after a contact time of 1 h, with removal up to 69% for Alg-rGO versus 21% for GAC toward RhB and up to 74% for Alg-GO versus 44% for GAC toward BP3. Adsorption efficiency was correlated to the oxidation degree of the 2D materials. Alg-GO-Lys and Alg-rGO were the most efficient sorbents for RhB (178 mg/g and 158 mg/g, respectively) taken as case study, with maximum adsorption capacity comparable to the value reported in literature for powder active carbon (190.84 mg/g), the benchmark for dyes adsorption. Moreover, the reusability of alginate-graphene beads after ethanol washing based regeneration was demonstrated.

Collectively, these results prove that the different GRM nanomaterials properties drive the adsorption selectivity and that the observed peculiarity are preserved also once the nanomaterials are embedded in the alginate gel matrix, this aiding the definition of guidelines for designing natural polymer-graphene nanomaterials composites for sustainable water treatment technologies.

CRediT authorship contribution statement

Francesca Tunioli: Methodology, Investigation. **Sara Khaliha:** Methodology, Investigation. **Sebastiano Mantovani:** Methodology, Investigation. **Antonio Bianchi:** Methodology, Investigation. **Alessandro Kovtun:** Investigation, Formal analysis. **Zhenyuan Xia:** Investigation. **Mohammad Sajad Sorayani Bafqi:** Investigation. **Matteo Calvaresi:** Investigation, Conceptualization. **Tainah D. Marforio:** Investigation. **Burcu Saner Okan:** Investigation, Validation. **Vincenzo Palermo:** Conceptualization, Validation. **Maria Luisa Navacchia:** Investigation, Formal analysis. **Manuela Melucci:** Conceptualization, Validation, Writing – original draft.

Declaration of Competing Interest

The authors declare the following financial interests/personal relationships which may be considered as potential competing interests: Manuela Melucci reports financial support was provided by Consiglio Nazionale delle Ricerche.

Data Availability

No data was used for the research described in the article.

Acknowledgment

This work was supported by the EU-project 825207 ‘GO-FOR-WATER’.

Appendix A. Supporting information

Supplementary data associated with this article can be found in the online version at doi:10.1016/j.jece.2023.109566.

References

[1] https://sdgs.un.org/goals.
[2] https://ec.europa.eu/info/law/better-regulation/initiatives/com-2017–753_en.
[3] S. Schulze, D. Zahn, R. Montes, R. Rodil, J.B. Quintana, T.P. Knepper, T. Reemtsma, U. Berger, Occurrence of emerging persistent and mobile organic contaminants in European water samples, Water Res 153 (2019) 80–90.
[4] S.D. Richardson, T.A. Ternes, Water analysis: emerging contaminants and current issues, Anal. Chem. 90 (1) (2018) 398–428.
[5] J.P. van der Hoek, C. Bertelkamp, A.R.D. Verliefde, N. Singhal, Drinking water treatment technologies in Europe: state of the art – challenges – research needs, J. Water Supply Res. T. Aqua 63 (2) (2013) 124–130.
[6] L. Malaeb, G.M. Ayoub, Reverse osmosis technology for water treatment: state of the art review, Desalination 267 (1) (2011) 1–8.
[7] F. Derbyshire, M. Jagtoyen, R. Andrews, A. Rao, I. Martin-Gullon, E. Grulke, Carbon materials in environmental applications, Chem. Phys. Carbon 27 (2000) 1–66.
[8] M. Melucci, E. Treossi, L. Ortolani, G. Giambastiani, V. Morandi, P. Klar, C. Casiraghi, P. Samorì, V. Palermo, Facile covalent functionalization of graphene oxide using microwaves: bottom-up development of functional graphitic materials, J. Mater. Chem. 20 (41) (2010) 9052–9060.
[9] M. Melucci, M. Durso, M. Zambianchi, E. Treossi, Z.-Y. Xia, I. Manet, G. Giambastiani, L. Ortolani, V. Morandi, F. De Angelis, V. Palermo, Graphene–organic hybrids as processable, tunable platforms for pH-dependent photoemission, obtained by a new modular approach, J. Mater. Chem. 22 (35) (2012) 18237–18243.
[10] M. Durso, A.I. Borrachero-Conejo, C. Bettini, E. Treossi, A. Scida, E. Saracino, M. Gazzano, M. Christian, V. Morandi, G. Tuci, G. Giambastiani, L. Ottaviano, F. Perrozzi, V. Benfenati, M. Melucci, V. Palermo, Biomimetic graphene for enhanced interaction with the external membrane of astrocytes, J. Mater. Chem. B 6 (33) (2018) 5335–5342.
[11] S. Khaliha, T.D. Marforio, A. Kovtun, S. Mantovani, A. Bianchi, M. Luisa Navacchia, M. Zambianchi, L. Bocchi, N. Boulanger, A. Iakunkov, M. Calvaresi, A.V. Talyzin, V. Palermo, M. Melucci, Defective graphene nanosheets for drinking water purification: adsorption mechanism, performance, and recovery, FlatChem (2021) *29*.
[12] S. Mantovani, S. Khaliha, L. Favaretto, C. Bettini, A. Bianchi, A. Kovtun, M. Zambianchi, M. Gazzano, B. Casentini, V. Palermo, M. Melucci, Scalable synthesis and purification of functionalized graphene nanosheets for water remediation, Chem. Commun. 57 (31) (2021) 3765–3768.
[13] L. Lombardi, A. Kovtun, S. Mantovani, G. Bertuzzi, L. Favaretto, C. Bettini, V. Palermo, M. Melucci, M. Bandini, Visible-light assisted covalent surface functionalization of reduced graphene oxide nanosheets with Arylazo sulfones, Chem. Eur. J. 28 (2022) 26.
[14] Pintus, A.; Mantovani, S.; Kovtun, A.; Bertuzzi, G.; Bandini, M.; Melucci, M., Recyclable GO-Arginine Hybrids for CO2 Fixation into Cyclic Carbonates. Chem. Eur. J. (Acepted Author Manuscript).
[15] N. Yousefi, X. Lu, M. Elimelech, N. Tufenkji, Environmental performance of graphene-based 3D macrostructures, Nat. Nanotechnol. 14 (2) (2019) 107–119.

[16] G. Crini, Non-conventional low-cost adsorbents for dye removal: a review, Bioresour. Technol. 97 (2006) 1061–1085.
[17] F. Perreault, A. Fonseca de Faria, M. Elimelech, Environmental applications of graphene-based nanomaterials, Chem. Soc. Rev. 44 (16) (2015) 5861–5896.
[18] O. Suárez-Iglesias, S. Collado, P. Oulego, M. Díaz, Graphene-family nanomaterials in wastewater treatment plants, J. Chem. Eng. 313 (2017) 121–135.
[19] S. Khaliha, A. Bianchi, A. Kovtun, F. Tunioli, A. Boschi, M. Zambianchi, D. Paci, L. Bocchi, S. Valsecchi, S. Polesello, A. Liscio, M. Bergamini, M. Brunetti, M. Luisa Navacchia, V. Palermo, M. Melucci, Graphene oxide nanosheets for drinking water purification by tandem adsorption and microfiltration, Sep. Purif. Technol. 300 (2022), 121826.
[20] M.R. Gandhi, S. Vasudevan, A. Shibayama, M. Yamada, Graphene and graphene-based composites: a rising star in water purification - a comprehensive overview, ChemistrySelect 1 (15) (2016) 4358–4385.
[21] K. Thakur, B. Kandasubramanian, Graphene and graphene oxide-based composites for removal of organic pollutants: a review, J. Chem. Eng. Data 64 (3) (2019) 833–867.
[22] M. Zambianchi, M. Durso, A. Liscio, E. Treossi, C. Bettini, M.L. Capobianco, A. Aluigi, A. Kovtun, G. Ruani, F. Corticelli, M. Brucale, V. Palermo, M. L. Navacchia, M. Melucci, Graphene oxide doped polysulfone membrane adsorbers for the removal of organic contaminants from water, J. Chem. Eng. 326 (2017) 130–140.
[23] M. Zambianchi, S. Khaliha, A. Bianchi, F. Tunioli, A. Kovtun, M.L. Navacchia, A. Salatino, Z. Xia, E. Briñas, E. Vázquez, D. Paci, V. Palermo, L. Bocchi, B. Casentini, M. Melucci, Graphene oxide-polysulfone hollow fibers membranes with synergic ultrafiltration and adsorption for enhanced drinking water treatment, J. Membr. Sci. 658 (2022), 120707.
[24] A. Kovtun, A. Bianchi, M. Zambianchi, C. Bettini, F. Corticelli, G. Ruani, L. Bocchi, F. Stante, M. Gazzano, T.D. Marforio, M. Calvaresi, M. Minelli, M.L. Navacchia, V. Palermo, M. Melucci, Core-shell graphene oxide-polymer hollow fibers as water filters with enhanced performance and selectivity, Faraday Discuss. 227 (2021) 274–290.
[25] M. Zambianchi, A. Aluigi, M.L. Capobianco, F. Corticelli, I. Elmi, S. Zampolli, F. Stante, L. Bocchi, F. Belosi, M.L. Navacchia, M. Melucci, Polysulfone hollow porous granules prepared from wastes of ultrafiltration membranes as sustainable adsorbent for water and air remediation, Adv. Sustain. Syst. 1 (7) (2017), 1700019.
[26] A. Kovtun, M. Zambianchi, C. Bettini, A. Liscio, M. Gazzano, F. Corticelli, E. Treossi, M.L. Navacchia, V. Palermo, M. Melucci, Graphene oxide-polysulfone filters for tap water purification, obtained by fast microwave oven treatment, Nanoscale 11 (47) (2019) 22780–22787.
[27] A. Kovtun, E. Campodoni, L. Favaretto, M. Zambianchi, A. Salatino, S. Amalfitano, M.L. Navacchia, B. Casentini, V. Palermo, M. Sandri, M. Melucci, Multifunctional graphene oxide/biopolymer composite aerogels for microcontaminants removal from drinking water, Chemosphere 259 (2020), 127501.
[28] S.J. Ajeel, A.A. Beddai, A.M.N. Almohaisen, Preparation of alginate/graphene oxide composite for methylene blue removal, Mater. Today.: Proc. 51 (2022) 289–297.
[29] S. Mantovani, S. Khaliha, T.D. Marforio, A. Kovtun, L. Favaretto, F. Tunioli, A. Bianchi, G. Petrone, A. Liscio, V. Palermo, M. Calvaresi, M.L. Navacchia, M. Melucci, Facile high-yield synthesis and purification of lysine-modified graphene oxide for enhanced drinking water purification, Chem. Commun. 58 (70) (2022) 9766–9769.
[30] S. Mantovani, T.D. Marforio, S. Khaliha, A. Pintus, A. Kovtun, F. Tunioli, L. Favaretto, A. Bianchi, M.L. Navacchia, V. Palermo, M. Calvaresi, M. Melucci, Amino acid-driven adsorption of emerging contaminants in water by modified graphene oxide nanosheets, Environ. Sci.: Water Res. Technol. (2023).
[31] H. Zhao, X.-K. Ouyang, L.-Y. Yang, Adsorption of lead ions from aqueous solutions by porous cellulose nanofiber–sodium alginate hydrogel beads, J. Mol. Liq. 324 (2021), 115122.
[32] J. Shen, X. Xu, X.-k Ouyang, M.-c Jin, Adsorption of Pb(II) from aqueous solutions using nanocrystalline cellulose/sodium alginate/K-carrageenan composite hydrogel beads, J. Polym. Environ. 30 (5) (2022) 1995–2006.
[33] L. Fan, Y. Lu, L.-Y. Yang, F. Huang, X.-k Ouyang, Fabrication of polyethylenimine-functionalized sodium alginate/cellulose nanocrystal/polyvinyl alcohol core–shell microspheres ((PVA/SA/CNC)@PEI) for diclofenac sodium adsorption, J. Colloid Interface Sci. 554 (2019) 48–58.
[34] E. Platero, M.E. Fernandez, P.R. Bonelli, A.L. Cukierman, Graphene oxide/alginate beads as adsorbents: influence of the load and the drying method on their physicochemical-mechanical properties and adsorptive performance, J. Colloid Interface Sci. 491 (2017) 1–12.
[35] W.M. Algothmi, N.M. Bandaru, Y. Yu, J.G. Shapter, A.V. Ellis, Alginate-graphene oxide hybrid gel beads: an efficient copper adsorbent material, J. Colloid Interface Sci. 397 (2013) 32–38.
[36] M. Majdoub, A. Amedlous, Z. Anfar, A. Jada, N. El Alem, Engineering of amine-based binding chemistry on functionalized graphene oxide/alginate hybrids for simultaneous and efficient removal of trace heavy metals: Towards drinking water, J. Colloid Interface Sci. 589 (2021) 511–524.
[37] Y. Fei, Y. Li, S. Han, J. Ma, Adsorptive removal of ciprofloxacin by sodium alginate/graphene oxide composite beads from aqueous solution, J. Colloid Interface Sci. 484 (2016) 196–204.
[38] Y. Sun, T. Zhou, W. Li, F. Yu, J. Ma, Amino-functionalized alginate/graphene double-network hydrogel beads for emerging contaminant removal from aqueous solution, Chemosphere 241 (2020), 125110.
[39] J. Wang, R.M. Wolf, J.W. Caldwell, P.A. Kollman, D.A. Case, Development and testing of a general amber force field, J. Comput. Chem. 25 (9) (2004) 1157–1174.
[40] D.A. Case, R. M, D.S. Cerutti, T.E. Cheatham III, T.A. Darden, R.E. Duke, T.J. Giese, H. Gohlke, A.W. Goetz, N. Homeyer, S. Izadi, P. Janowski, J. Kaus, A. Kovalenko, T. S. Lee, S. LeGrand, P. Li, C. Lin, T. Luchko, R. Luo, B. Madej, D. Mermelstein, K. M. Merz, G. Monard, H. Nguyen, H.T. Nguyen, I. Omelyan, A. Onufriev, D.R. Roe, A. Roitberg, C. Sagui, C.L. Simmerling, W.M. Botello-Smith, J. Swails, R.C. Walker, J. Wang, R.M. Wolf, X. Wu, L. Xiao, P.A. Kollman, AMBER, University of California, San Francisco, 2016.
[41] B.R. Miller, I.I.I. McGee, T.D. Swails Jr, J.M. Homeyer, N. Gohlke, H. Roitberg, A. E, MMPBSA.py: an efficient program for end-state free energy calculations, J. Chem. Theory Comput. 8 (9) (2012) 3314–3321.
[42] I. Berktas, A.N. Ghafar, P. Fontana, A. Caputcu, Y. Menceloglu, B.S. Okan, Facile synthesis of graphene from waste tire/silica hybrid additives and optimization study for the fabrication of thermally enhanced cement grouts, Molecules 25 (4) (2020) 886.
[43] M.M. Campos-Vallette, N.P. Chandía, E. Clavijo, D. Leal, B. Matsuhiro, I.O. Osorio-Román, S. Torres, Characterization of sodium alginate and its block fractions by surface-enhanced Raman spectroscopy, J. Raman Spectrosc. (2009) (n/a-n/a).
[44] S. Liu, Y. Wang, B. Wang, J. Huang, S. Deng, G. Yu, Regeneration of Rhodamine B saturated activated carbon by an electro-peroxone process, J. Clean. Prod. 168 (2017) 584–594.
[45] M. Kumar, G. Vijayakumar, R. Tamilarasan, Synthesis, characterization and experimental studies of nano Zn–Al–Fe3O4 blended alginate/Ca beads for the adsorption of rhodamin B, J. Polym. Environ. 27 (1) (2019) 106–117.
[46] W. Xiao, Z.N. Garba, S. Sun, I. Lawan, L. Wang, M. Lin, Z. Yuan, Preparation and evaluation of an effective activated carbon from white sugar for the adsorption of rhodamine B dye, J. Clean. Prod. 253 (2020), 119989.
[47] S.M. Al-Rashed, A.A. Al-Gaid, Kinetic and thermodynamic studies on the adsorption behavior of Rhodamine B dye on Duolite C-20 resin, J. Saudi Chem. Soc. 16 (2) (2012) 209–215.